Support information for:

Bifunctional and stable NiCoS/NiCoP bistratal electrocatalyst for 10.8%-efficient overall solar water splitting

Xiaoxue Zhou,[a] Ju Zhou,[a] Guanping Huang,[a] Ronglei Fan,[a,b] Sheng Ju,[a] Zetian Mi,[b] and Mingrong Shen[a] *

[a]*School of Physical Science and Technology, Jiangsu Key Laboratory of Thin Films, and Collaborative Innovation Center of Suzhou Nano Science and Technology, Soochow University, 1 Shizi street, Suzhou 215006, China*

[b] *Department of Electrical Engineering and Computer Science, Center for Photonics and Multiscale Nanomaterials, University of Michigan, 1301 Beal Avenue, Ann Arbor, MI, 48109, United States*

*E-mail: mrshen@suda.edu.cn

Experimental section

Materials

Cobalt chloride ($CoCl_2 \cdot 6H_2O$), nickel chloride ($NiCl_2 \cdot 6H_2O$), sodium hypophosphite ($NaH_2PO_2 \cdot H_2O$), ammonium chloride (NH_4Cl), hydrochloric acid (HCl) and thiourea were used as received. All reagents were of analytical grade and used without further purification.

Electrodeposition of NCP and NCS

Before the electrodeposition of NCP, the NF substrate surface was cleaned ultrasonically in 20% HCl solution to remove surface oxides, and was then ultrasonically cleaned with ethanol and DI water to remove surface pollutants. The electrodeposition solution consisted of $CoCl_2 \cdot 6H_2O$ (0.2 M), $NiCl_2 \cdot 6H_2O$ (0.2 M), $NaH_2PO_2 \cdot H_2O$ (0.2 M) and NH_4Cl (0.25 M) with DI water. For the three-electrode electrodeposition system, NFs serve as the working electrode, graphite rod as the counter electrode, and Ag/AgCl electrode as the reference electrode. Electrodeposition of NCP was attained via constant current with 10 mA/cm^2 current density. Different NCP samples were fabricated by controlling the electrodeposition times (20, 40, 60, and 90 min). After electrodeposition, these samples were rinsed with deionized water and dried in a vacuum oven.

NCS films were fabricated also by a electrodeposition method on NFs or NCP/NFs, which was carried out by repeated potential cycling between 0.15 and -1.25 V versus reverse hydrogen electrode (*vs.* RHE) at 5 mV/s. The electrolytes were 0.5 M aqueous solutions of thiourea containing 2.5 mM $NiCl_2 \cdot 6H_2O$ and 2.5mM $CoCl_2 \cdot 6H_2O$. N_2 gas with a purity of 99.9% was purged through the electrolyte for 30 min before the deposition and the flow was maintained throughout the deposition process. Different NCS samples were fabricated by controlling the electrodeposition cycles (5, 10 and 15 cycles). The deposited electrodes were rinsed in water and dried overnight under vacuum.

Physical Characterization and Electrochemical Studies

The morphology of sample surface was analyzed by field-emission scanning electron microscope (SEM) (SU8010, Hitachi). The transmission electron microscope (TEM) analysis was conducted by a Tecnai G220 (S-TWIN, FEI) operating at 200 kV. X-ray photoelectron spectroscopy (XPS) measurements were performed at room temperature using a spectrometer hemispherical analyzer (ESCALAB 250Xi, Thermo). The electrochemical performance for HER and OER was conducted in a three-electrode configuration in a solution containing 1 M NaOH (Sinopharm Chemical Reagent Co., Ltd., Analytical reagent, pH=13.6). The catalyst/NF was used as working electrode, Ag/AgCl (3 M KCl) as reference electrode, and graphite rod as counter electrode. The potentials were controlled using an electrochemical workstation (Vertex, Ivium Technologies) at a scan rate of 20 mV/s and re-scaled to the potential according to the following equation: $V_{RHE} = V_{Ag/AgCl} + E(Ag/AgCl) + pH \times 0.059$ V, where E(Ag/AgCl) = 0.197 V. Electrochemical impedance spectroscopy (EIS) measurements were conducted at -0.15 V *vs.* RHE over the frequency range of 100 kHz to 0.10 Hz. iR-correction was applied for the HER and OER polarization curves. A typical value of 1.5-2 Ω was measured as the internal resistance. The Tafel slope is an important parameter to explain the electrocatalytic activity and kinetics of a given reaction and can be expressed as follows: [17]

$$\eta = a + \frac{2.3RT}{\alpha nF}\log j$$

where η is the overpotential, α is the transfer coefficient, n is the number of electrons involved in the reaction, F is the Faraday constant, j is the current density and the slope is given by 2.3RT/αnF. Electrochemical capacitance was measured using cyclic voltammetry (CV) measurements. The currents were measured in a narrow potential window that no faradaic processes were observed. CVs were collected at different scan rates: 20, 40, 60, 80, 100, 120, 140, 160 and 180 mV/s. The measured current in this non-Faradaic potential region should be mostly due to the charging of the double-layer. And the capacitive currents (i_{dl}) are the difference between two currents at 1.07 V *vs.* RHE. The overall water splitting test was performed in a two-electrode system in 1 M NaOH, with the working electrode lead of the workstation connecting to the one

NCS/NCP/NF electrode and the reference and the counter electrode lead of the workstation to the other NCS/NCP/NF electrode. The performance of overall water splitting was characterized by current density-potential (J-V) curves at a scan rate of 2 mV/s, 5 mV/s, 20 mV/s from 0 V to 2 V. When measuring the optical characteristics, a 300 W Xe lamp (Oriel, Newport Co.) with an IR cutoff filter was used as a light source. The light intensity was carefully maintained at 100 mW/cm^2, measured using an optical power meter (Newport Co.) just before the light enters into the PEC cell.

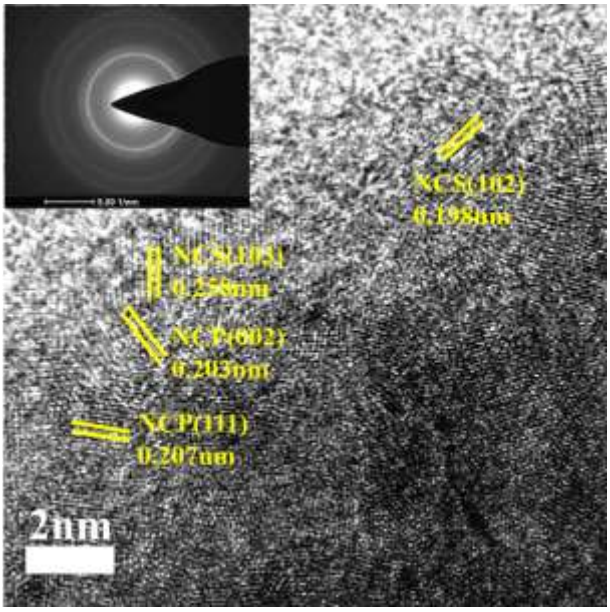

Figure S1. HRTEM image and (inset) SAED patterns of NCS/NCP.

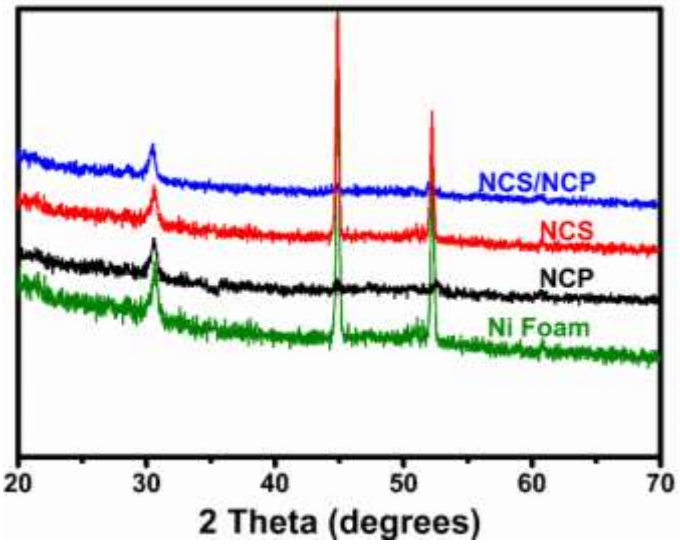

Figure S2. XRD spectra of (a) NF, (b) NCP/NF, (c) NCS/NF, (d) NCS/NCP/NF. Comparing with the pure Ni foam (NF), the XRD spectra for NCS/NF, NCP/NF and NCS/NCP/NF show no additional XRD peaks, indicating the poor crystallinity.

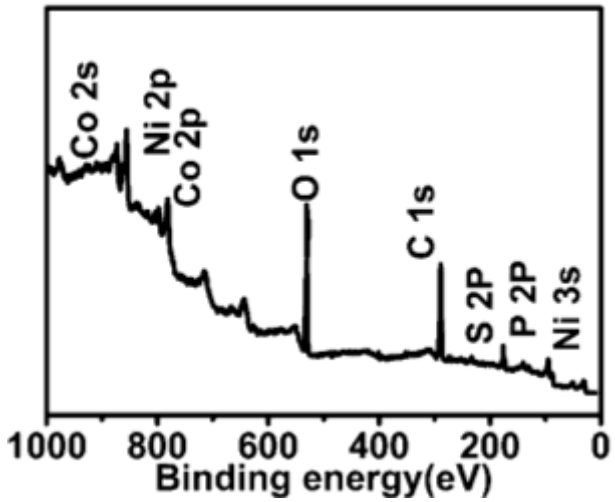

Figure S3. XPS spectrum of NCS/NCP/NF.

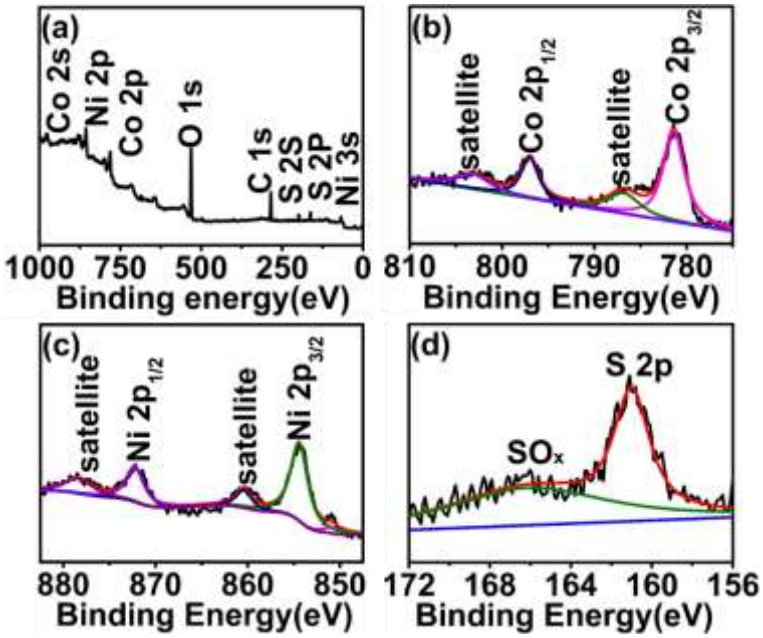

Figure S4. XPS spectra of NCS: (a) survey and high-resolution spectra of (b) Co 2p region, (c) Ni 2p region and (d) S 2p region.

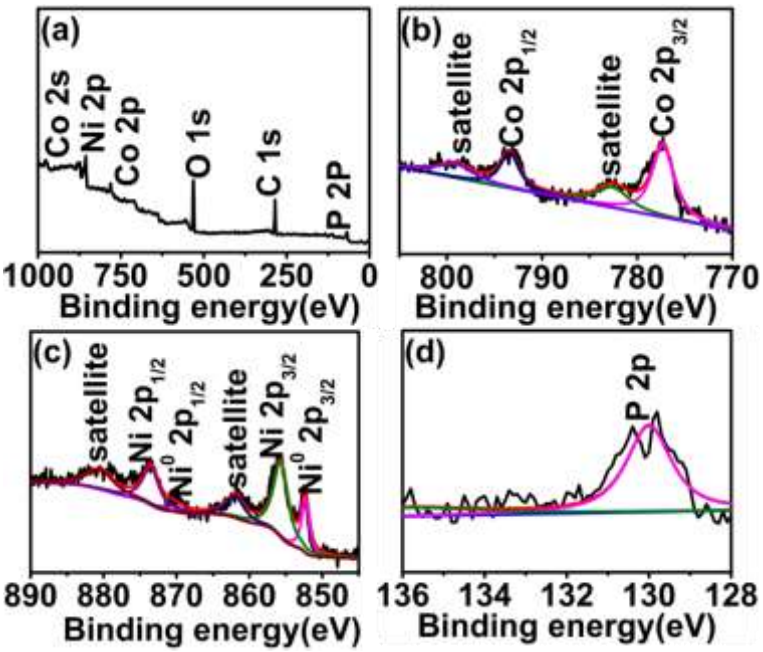

Figure S5. XPS spectra of NCP: (a) survey and high-resolution spectrum of (b) Co 2p region, (c) Ni 2p region and (d) P 2p region.

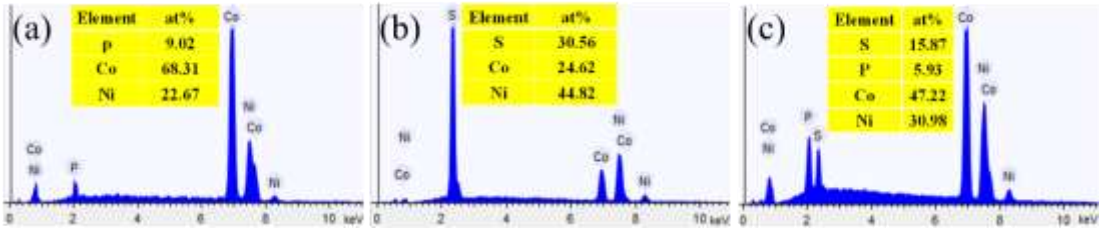

Figure S6. EDX of NCP, NCS, NCS/NCP. The corresponding atomic percentages are presented in the respective pictures.

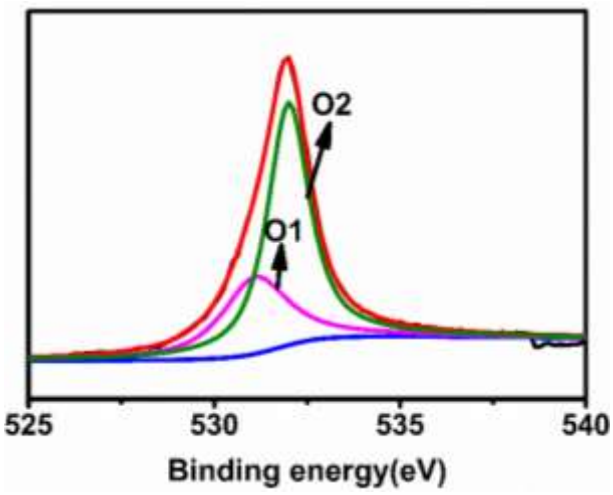

Figure S7. XPS O1s peak for NCS/NCP/NF sample.

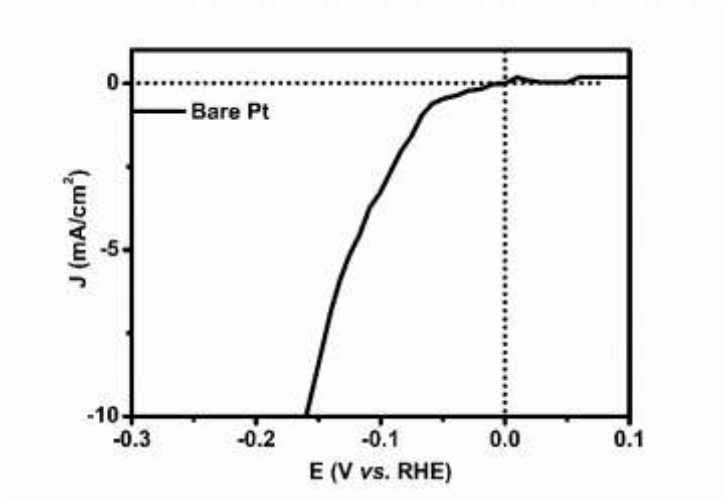

Figure S8. The PEC J-V measurements for the Pt as the working electrode. We can see that the cathodic current happens at 0V vs. RHE, confirming the detail potential of Ag/AgCl reference electrode is not deviated from 0.197 V.

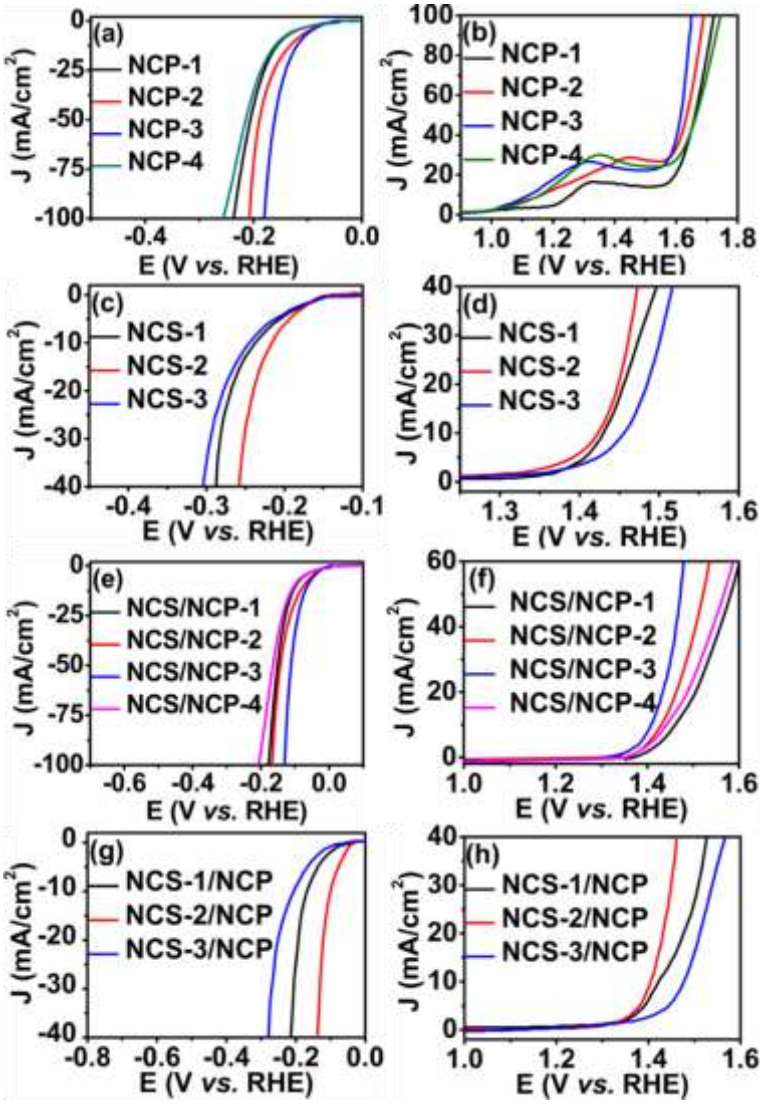

Figure S9. (a) HER and (b) OER polarization curves of NCP with different deposition time of 20, 40, 60 and 90 min, corresponding to NCP-1, NCP-2, NCP-3 and NCP-4. NCP-3 shows the best HER and OER catalytic activity. In the main text, NCP means NCP-3.

(c) HER and (d) OER polarization curves of NCS with different deposition cycles of 5, 10 and 15, corresponding to NCS-1, NCS-2 and NCS-3. NCS-2 presents the best HER and OER catalytic activity. In the main text, NCS means NCS-2.

(e) HER and (f) OER polarization curves of NCS-2/NCP(20, 40, 60 and 90 min). NCS-2/NCP-3 have the best HER and OER catalytic activity.

(g) HER and (h) OER polarization curves of NCS(5, 10 and 15 cycles)/NCP-3. Again, NCS-2/NCP-3 have the best HER and OER catalytic activity.

In the main text, NCS/NCP means NCS-2/NCP-3.

All the curves are iR-corrected.

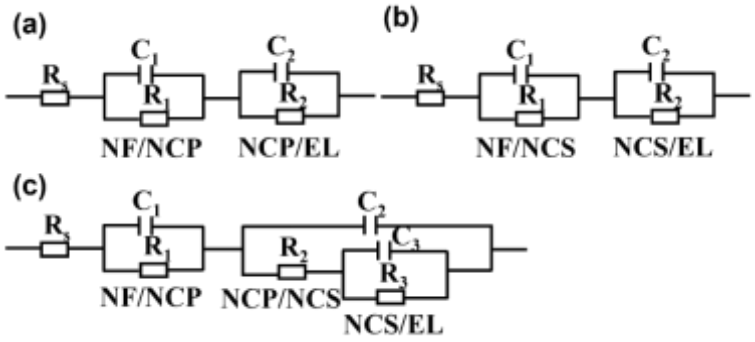

Figure S10. The equivalent circuit of (a) NCP/NF, (b) NCS/NF, (c) NCS/NCP/NF.

	R_S	R_1	R_2	R_3
NCP	1.73	0.29	8.78	\
NCS	1.61	0.41	7.19	\
NCS/NCP	1.72	0.30	0.23	2.16

Table S1. The fitting results for the transfer resistances using the equivalent circuit of Figure S10.

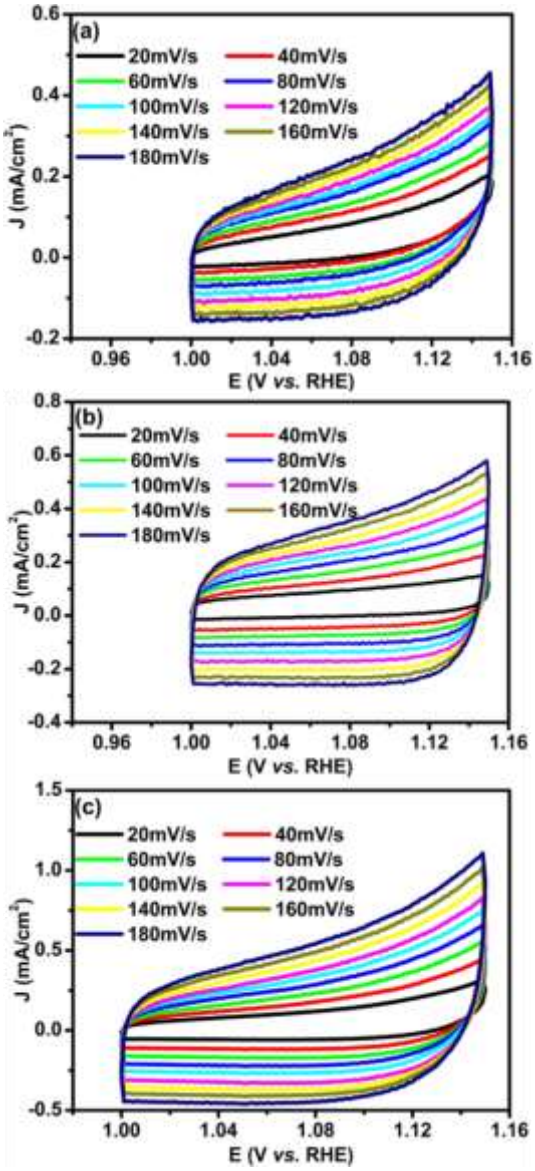

Figure S11. Typical CV curves of (a) NCP, (b) NCS and (c) NCS/NCP.

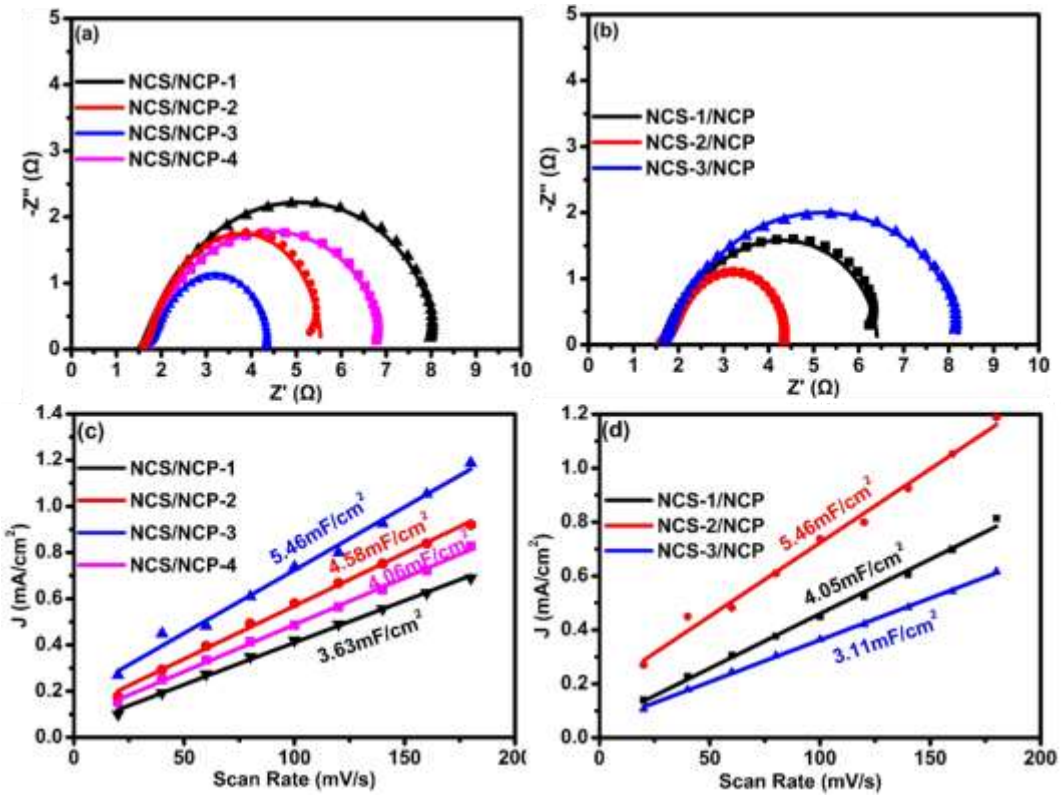

Figure S12. (a) EIS Nyquist plots of NCS/NCP-1, 2, 3, 4, on NFs. (b) EIS Nyquist plots of NCS-1, 2, 3/NCP on NFs. (c) and (d) the capacitive currents at 1.07 V *vs.* RHE as a function of scan rate.

	C_{dl} (mF)	ECSA (cm^2)
NCP	1.39	34.75
NCS	3.48	87
NCS/NCP	5.46	136.5
NCS/NCP-1	4.06	101.5
NCS/NCP-2	4.58	114.5
NCS/NCP-3	5.46	136.5
NCS/NCP-4	3.63	90.75
NCS-1/NCP	4.05	101.25
NCS-2/NCP	5.46	136.5
NCS-3/NCP	3.11	77.75

Table S2. The fitting results for the ECSA calculated based on ECSA= C_{dl}/C_s.

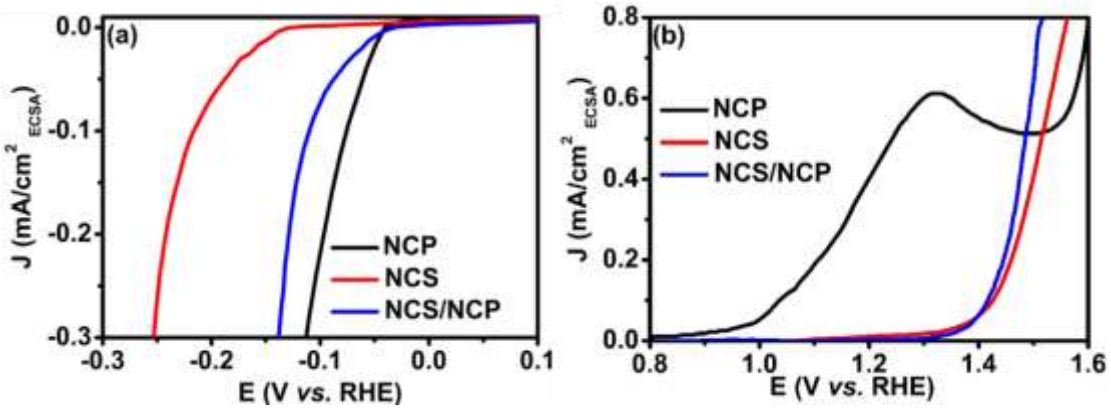

Figure S13. (a) HER and (b) OER polarization curves normalized by ECSA for the NCP, NCS, NCS/NCP catalysts.

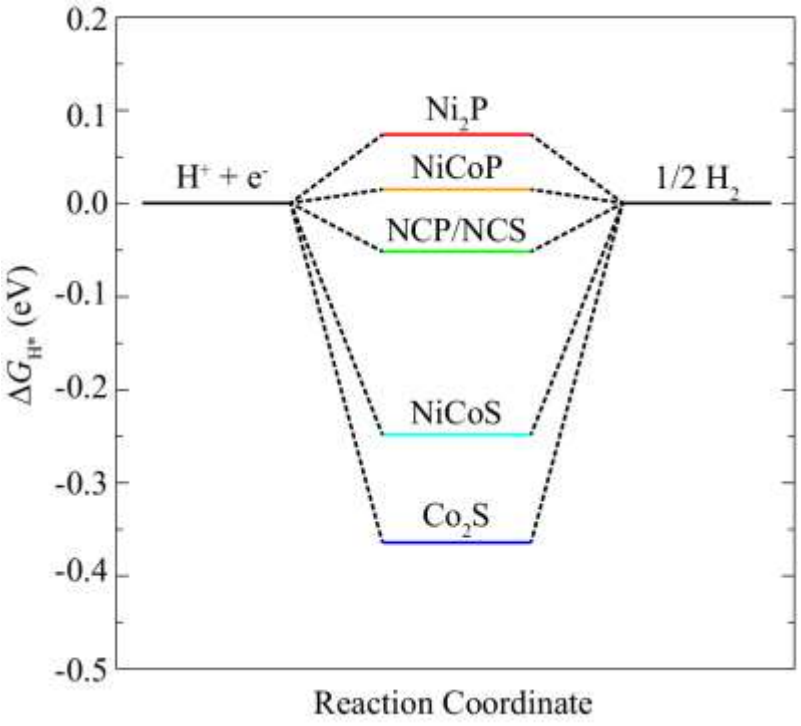

Figure S14. The calculated free-energy diagram of the HER at the equilibrium potential on the surface of various catalysts.

The Vienna ab initio simulation package (VASP) was used to perform the first-principles calculations [1,2]. The interaction between the atomic cores and electrons were described according to the projector augmented wave (PAW), with the plane wave cutoff of 500 eV [3]. The Generalized Gradient Approximation (GGA) with the Perdew–Burke–Ernzerhof (PBE) exchange–correlation functional was applied [4]. The NiCoP and NiCoS surfaces were modelled by using a supercell slab containing four atomic layers to eliminate the polarity with a vacuum gap of ~15 Å. A Monkhorst–Pack grid of 6×6×1 size was used to sample the surface Brillouin zone. The lowest two layers

were fixed and the other layers were fully relaxed. The convergence criterion for total energies was set to 10^{-5} eV.

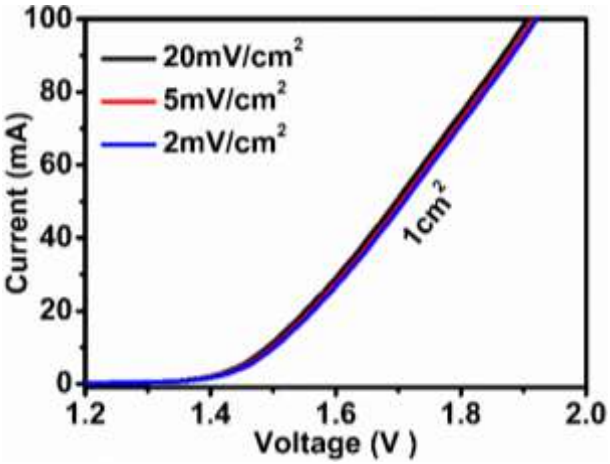

Figure S15. Current-voltage (I-V) characteristics for the overall electrocatalytic water splitting using NCS/NCP/NF for both the anode and cathode under different scan rates.

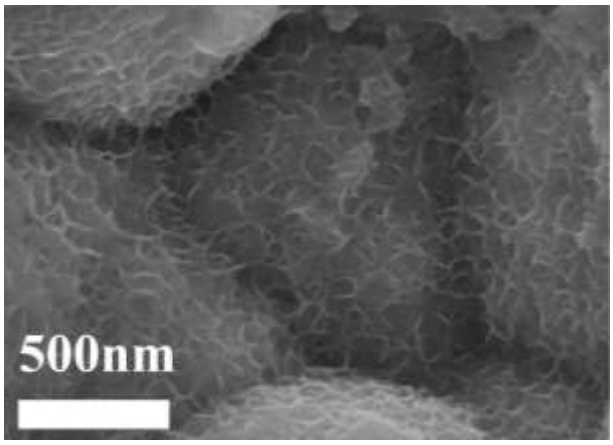

Figure S16. The surface morphology of the NCS/NCP/NF sample after long-term electrolysis.

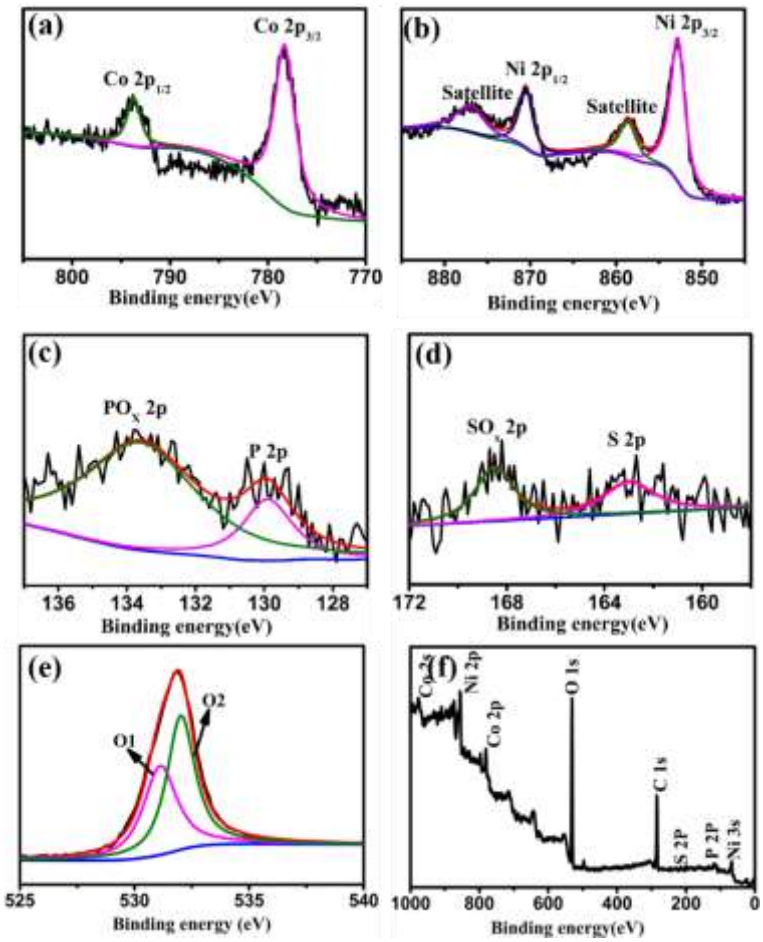

Figure S17. XPS spectra of NCS/NCP after long-term electrolysis: high-resolution spectrum of (a) Co 2p region, (b) Ni 2p region, (c) P 2p region, (d) S 2p region, (e) O 1s region and (f) survey.

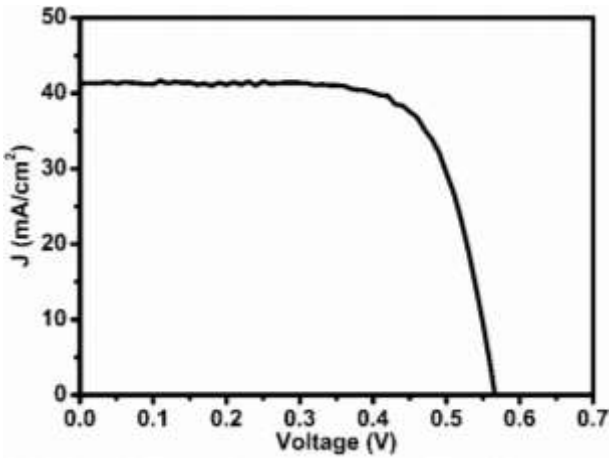

Figure S18. Current potential (I-V) characteristics of ordinary single-crystal Si solar cells.

Firstly, single solar cells were made. Single-crystalline p-Si wafers (1-3 Ω·cm specific resistance, Canadian Solar Inc.) were used for this work. The pyramid surface texture of both side was produced by a standard process of alkaline etching and then

the surface pn^+ junction was fulfilled by a standard process of phosphorus doping. After doping, an anti-reflection SiN_x layer and fritted Ag bar line were produced onto the n^+-Si emitter side. A fritted Al paste was screen-printed onto the rear surface. Finally, the samples were laser-cut into 1.5 × 1.5 cm^2.

Secondly, three solar cells are connected in series using Ag wires. One side is connected to Ag bar line of one solar cell, and another to Al back electrode of another solar cell. In order to form ohmic contacts, Ag wires were embedded in Ag paste when contacting. After Ag paste is dried completely, all the Al surfaces of three solar cells were adhered to a quartz plate (4 × 4 cm^2). At last, edges of the electrodes (except for the intended reaction area 3 × 1 cm^2) were sealed with an industrial epoxy (PKM12C-1, Pattex).

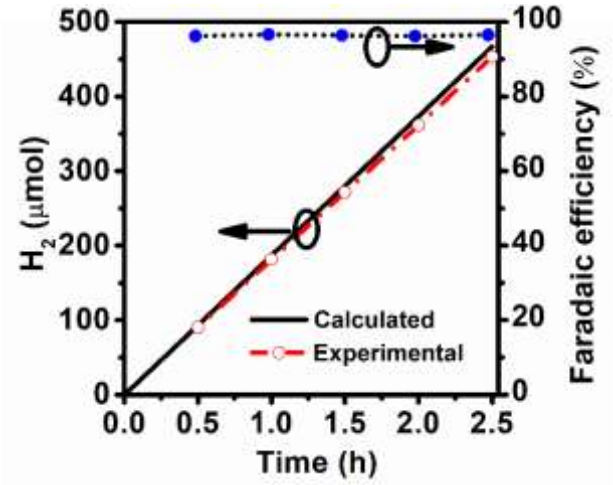

Figure S19. Hydrogen production production on time and the corresponding faradic efficiency for the NCS/NCP/NF as both the anode and cathode measured at 10 mA/cm^2.

Catalysts	Electrolyte	Overpotential	η_{STH}	Reference
NCS/NCP/NF	1 M KOH or NaOH	**1.49 V @ 10 mA/cm^2**	**10.8%**	**This work**
Ni-Co-S/NF//Ni-Co-P/NF		1.57 V @ 20 mA/cm^2	/	*J. Mater. Chem. A* **2018**, 6, 12506 -12514
NiFe inverse opal		1.76 V @ 10 mA/cm^2	9.54%	*Nano Energy* **2017,** 42, 1-7.
MoS_2/Ni_3S_2		1.56 V @ 10 mA/cm^2		*Angew. Chem.* **2016**, 128, 6814 - 6819.
FeP/Ni_2P		1.42 V @ 10 mA/cm^2		*Nature communications* **2018**, 9, 2551 (1-7).
$NiFe/NiCo_2O4/NF$		1.67 V @ 10 mA/cm^2		*Adv. Funct. Mater.* **2016**,

				26, 3515 - 3523.
NiSe/Ni_3Se_2		1.6 V @ 10 mA/cm^2		*Adv. Mater. Interfaces* **2018,** 5 (8), 1701507.

Table S3. Comparison of the catalytic activities of some recent Ni-based catalysts.

REFERENCES

(1) Kresse G.; Furthmüller J., Efficient iterative schemes for *ab initio* total-energy calculations using a plane-wave basis set. *Phys. Rev. B* **1996**, *54* (16), 11169.

(2) Kresse G.; Furthmüller J., Efficiency of ab-initio total energy calculations for metals and semiconductors using a plane-wave basis set. *Comput. Mater. Sci.* **1996**, *6* (1), 15-50.

(3) Kresse G.; Joubert D., From ultrasoft pseudopotentials to the projector augmented-wave method. *Phys. Rev. B* **1999**, *59* (3), 1758.

(4) Perdew J. P.; Burke K.; Ernzerhof M., Generalized Gradient Approximation Made Simple. *Phys. Rev. Lett.* **1996**, *77* (18), 3865.